Monte Carlo Methods for Including Calibration Uncertainties in Model Fitting Analyses

Jeremy J. Drake[a], Peter Ratzlaff[a], Vinay Kashyap[a], Richard Edgar[a], Rima Izem[b], Diab Jerius[a], Herman Marshall[c], Aneta Siemiginowska[a] and Alexey Vikhlinin[a]

[a]Smithsonian Astrophysical Observatory, Cambridge MA 02138
[b]Department of Statistics, Harvard University, Cambridge, MA 02138
[c]MIT Kavli Institute for Astronomy and Space Research, Cambridge, MA 02139

SUMMARY

- Instrument response uncertainties almost universally ignored in astrophysical X-ray data analyses, yet for good quality observations can be dominant source of error.
- Response uncertainties are *correlated*; both understanding and specifying the uncertainties is technically challenging. Moreover, **there is no standard set of procedures for incorporating complicated correlated systematic uncertainties in non-linear parameter estimation (eg XSPEC fitting): the approaches used for treating independent errors simply do not apply.**
- We have developed Monte Carlo methods to treat calibration uncertainties for the *Chandra* High Resolution Mirror Assembly (HRMA) and Advanced CCD Imaging Spectrograph (ACIS). The code and ancilliary data will be released to *Chandra Users* upon acceptance for publication of the article describing this work. CIAO *Sherpa* methods are also under development to utilise these techniques (see accompanying poster by Kashyap et al).

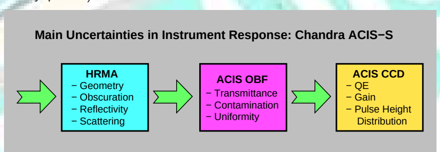

METHODS

Construct different realisations of instrument response by a combination of (1) randomly varying input parameters describing subassembly performance and (2) random multiplicative *perturbation functions*, $\mu(E)$, designed to sample subassembly responses with their assessed uncertainties (Fig. 1). Adopt "curtailed Gaussian" probability distribution $P(\sigma)$ for Monte Carlo draws (Fig. 1a). The different subassemblies were treated as follows:

HRMA On-Axis: A combination of perturbation functions, $\mu_H(E)$, running within prominent Ir edges, and raytrace-derived effective areas sampling the effects of different hydrocarbon contamination layers with the measured range of allowed values (Fig. 2).

HRMA Vignetting Function: For off-axis angles θ (in arcmin) the area perturbation function was multiplied by a combination of a fractional uncertainty of the azimuthally-averaged vignetting function, $V(\theta)$, and an expression involving the ratio of Debye-Waller to perfect mirror reflectivities:
$\mu_v(E,\theta) = P(\sigma_v)(1-\bar{V(\theta)}) + \theta P(\sigma_s)(1-R_{DW}/R)$; $\sigma_v, \sigma_s = 0.2$.

ACIS OBF and Contamination Layer: OBF transmittance uncertainty employed perturbation functions, $\mu_{OBF}(E)$, between C-N and N-O edges, and O-10 keV constrained by different allowed maximum deviations and relative edge transmittance discontinuity errors. The contamination perturbation function is:
$\mu_{CL}(E) = e^{-P(\sigma_C)\tau_C + P(\sigma_O)\tau_O + P(\sigma_F)\tau_F + P(\sigma_{Fl})\tau_{Fl}}$; $\mu_{CL}(0.7keV) < 0.05$
where σ_C, σ_O, σ_F and σ_{Fl} are the fractional uncertainties in the optical depths C, O, F and Fluffium at a fiducial date (2003.29).

ACIS QE: QE uncertainty base on combination of perturbation functions, $\mu_{QE}(E)$, with boundaries at O and Si K edges and ACIS QE model predictions for uncertainties of 13% in CCD depletion depth and 20% in SiO_2 thickness.

ACIS Gain and Pulse Height Distribution: Program `calcrmf2` used to generate CCD Gain and pulse height response matrix files (RMF) for $P(\sigma_G)$ variations in gain and pulse height width; σ_G =1% @0.7 keV, 0.5% @1.5 keV, and 0.2% @≥ 4 keV.

ESTIMATING EFFECTS OF CALIBRATION UNCERTAINTIES

Perturb nominal effective area, $A(E)$, with combined perturbation functions, $\mu(E)$, to make $A\prime(E)$ (Fig. 3):

$$A'(E) = \mu_H(E)\mu_V(E)\mu_{CL}(E)\mu_{OBF}(E)\mu_{QE}(E)A(E)$$

For each effective area and RMF, find the parameters of the best-fit model for a synthetic *Chandra* ACIS observation computed using the nominal instrument response. Compare with parameters found from fits to 1000 synthetic spectra differing only by Poisson noise and generated using the nominal area and RMF (Figs. 4 and 5). This step utilized the XSPEC fitting engine and investigated Blackbody, optically-thin thermal plasma, and power law continuum models. **Repeat 1000 times.**

- Limiting accuracy of *Chandra* ACIS reached in spectra with $\sim 10^4$ counts. Beyond this, errors in in best-fit parameters due to calibration uncertainties completely dominate those due to photon noise.

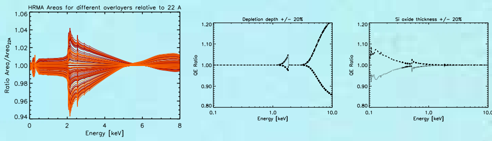

Figure 2. Left: Illustration of the relative change in the HRMA effective area caused by different hydrocarbon contamination layers. The range shown corresponds to the nominal adopted 22 ± 6 Å layer thickness. **Middle:** Relative changes in the model ACIS S3 QE caused by ±20% differences in the model CCD depletion depth (note that ±13 % was adopted here, which corresponds to a range of about ±10% in the QE at 10 keV). **Right:** QE changes caused by the adopted ±20% differences in CCD SiO_2 thickness.

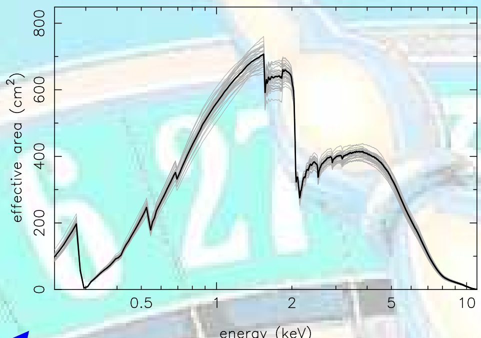

Figure 3. The nominal "seed" *Chandra* ACIS-S effective area (black) compared with a sample of 30 effective areas generated using the Monte Carlo modification method described in the text (grey).

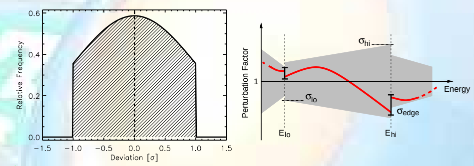

Figure 1. Left: Truncated normal distribution (product of a Gaussian with variance σ^2 and a rectangular Step function with unit density between $\pm\sigma$), $P(\sigma)$, representing the distribution of calibration uncertainties used in the perturbation function and Monte Carlo draws. **Right:** Illustration of a *perturbation function* segment used to apply random deviations from a nominal subassembly response within a given energy range. Within each energy range, E_{lo}–E_{hi}, a random low-order polynomial (≤ 3) is generated that is constrained to lie within the grey shaded region defined by the uncertainties σ_{lo} and σ_{hi}, and also to join up with neighbouring segments within the edge constraints σ_{edge}. The deviation from unity for a large sample of vectors corresponds to $P(\sigma)$.

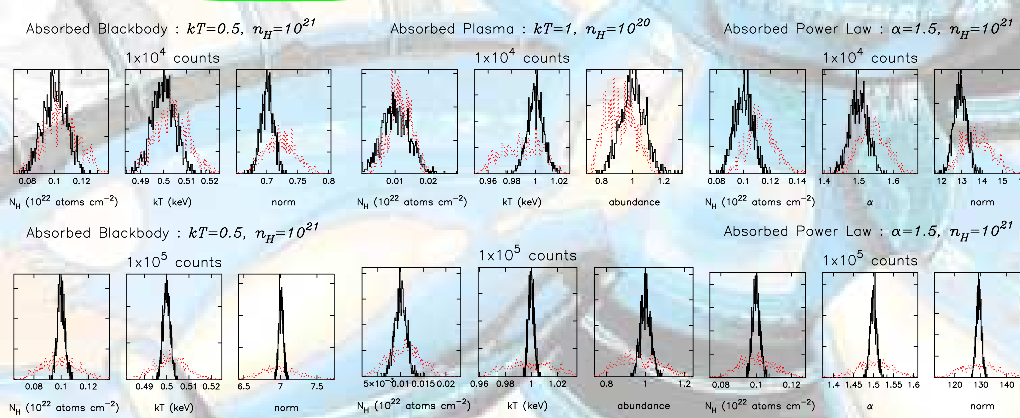

Figure 4. Example frequency distributions of best-fit parameters obtained for typical blackbody, thermal plasma and powerlaw models from XSPEC for synthetic data sets containing 10^4 (upper panels) and 10^5 (lower panels). Black histograms are distributions resulting from 1000 Monte Carlo samplings of the synthetic data allowing Poisson noise variations alone. Red histograms are the distributions of parameters resulting from fits to a single synthetic data set using 1000 Monte Carlo-generated effective areas and response matrices.

Figure 5. Modes and highest posterior density ±95% confidence intervals obtained for the blackbody, thermal plasma and powerlaw models investigated using XSPEC for synthetic data sets containing 10^5 counts. The y-axes correspond in all cases to the ratio of the input parameter to that retrieved in the model fit. Black error bars correspond to 1000 Monte Carlo samplings of the synthetic data and show the effects of Poisson noise variations alone. Dashed error bars correspond to fits to a single synthetic data set using 1000 Monte Carlo-generated effective areas and response matrices.